Spectroscopy and Dynamics of the 7,7,8,8-Tetracyanoquinodimethane Radical Anion

Gareth M. Roberts,[a] Julien Lecointre,[a] Daniel A. Horke[a] and Jan R. R. Verlet*[a]

Received (in XXX, XXX) Xth XXXXXXXXX 200X, Accepted Xth XXXXXXXXX 200X
First published on the web Xth XXXXXXXXX 200X
DOI: 10.1039/b000000x

The photoelectron spectrum of the 7,7,8,8-tetracyanoquinodimethane (TCNQ) radical anion has been measured at 3.1 eV. Additionally, the ultrafast relaxation dynamics of the first excited state (1^2B_{3u}) of $TCNQ^-$ have been studied using time-resolved photoelectron spectroscopy, which reveals that it undergoes internal conversion back to the ground state ($^2B_{2g}$) with an associated lifetime of 650 fs and shows evidence of coherent nuclear motion.

Introduction

Following the observations in the early 60's that certain organic salts of the 7,7,8,8-tetracyanoquinodimethane (TCNQ) radical anion show electrical conductivity approaching that of bulk metals,[1,2] the field of charge-transfer (CT) complexes and the chemists' ability to develop efficient conductive organic complexes has become one of the corner-stone goals of modern chemistry.[3,4] TCNQ is a planar organic molecule with D_{2h} symmetry (see Fig. 1) and has a conjugated π-system, which, together with the cyano groups, leads to a high electron affinity. In the condensed phase, TCNQ based CT salts owe their high conductivities to a π-π stacking motif, resulting in the spatial and energetic overlap between their respective π-orbitals. This is exemplified by the complex of the tetrathiofulvane (TTF) radical cation and the TCNQ radical anion, which is commonly regarded as the benchmark CT complex.[5] At a temperature of 66 K it possesses a conductivity of $1.47\times10^4\ \Omega^{-1}\ cm^{-1}$, approaching that of copper at room temperature ($6\times10^5\ \Omega^{-1}\ cm^{-1}$) and for this reason the term "organic metal" has become widely used to describe these highly conductive organic salts.[6]

TCNQ based complexes remain at the focus of much ongoing interdisciplinary research and there has been a large amount of effort invested into the derivatisation of complexes such as TTF-TCNQ with the aim of increasing their conductivities to that of bulk metals.[6,7] This includes, for example, the covalent linking of donor and acceptor molecules for application to high efficiency solar cells.[8,9] To date, enhancing the conductive properties of these complexes has proved to be somewhat empirical. Additionally, salts of $TCNQ^-$ with alkali metal cations possess interesting spin lattice properties at low temperatures (<66 K),[10] causing a dramatic conductor to insulator transition. More generally, molecules derived from TCNQ have found wide ranging applications in, for example: non-linear optics,[11] liquid crystal displays[12] and organic light-emitting devices.[13]

Despite the broad interest in TCNQ complexes, it is rather surprising that there are virtually no experimental studies into the electronic structure and relaxation dynamics of the fundamental $TCNQ^-$ building block. Here we report the photoelectron spectrum of the isolated TCNQ radical anion at 3.1 eV, which provides insight into the structure of the anion and the neutral. Furthermore, we study the ultrafast relaxation dynamics of photo-excited $TCNQ^-$, yielding molecular level information about the flow of energy in the molecule. The detailed knowledge of the molecular and electronic structure, as well as relaxation dynamics gained through such experiments, are prerequisites to further our understanding of not only the CT mechanism, but to ultimately guide the development of new CT complexes and other novel materials based on TCNQ.

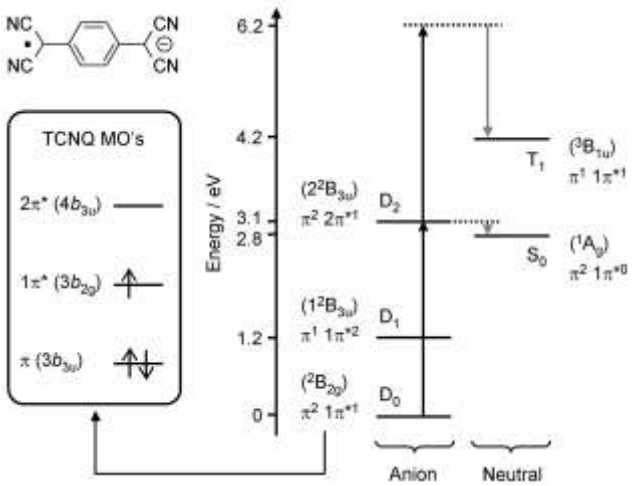

Fig. 1 State energy level diagram for the anion and neutral states of TCNQ. Presented in parentheses are the term symbols associated with each state and their electronic configurations shown below. Solid black vertical arrows indicate one- and two-photon detachment at 3.1 eV and grey vertical arrows represent the subsequent electron kinetic energies for the two processes. The molecular structure of the TCNQ radical anion is shown on the left as well as its molecular orbitals, with orbital symmetries shown in parentheses.

The electron affinity of TCNQ has been determined to be 2.8 ± 0.1 eV[14] through collisions of neutral TCNQ with fast caesium atoms. The gas-phase photodetachment spectrum, recorded by Brauman and co-workers, reveals strong absorptions around 3.1 eV and 1.2 eV,[15] and the spectrum closely resembles the absorption spectrum of $TCNQ^-$ in solution.[16] The lower energy band is a broad feature (1.2 – 2.2 eV) that exhibits two dominant vibrational progressions

arising from a core-excitation involving a $\pi^1 1\pi^{*2} \leftarrow \pi^2 1\pi^{*1}$ transition as indicated in Fig. 1, where we use the labelling D_0, D_1 and D_2 to indicate the doublet states of the anion and S_0 and T_1 for the ground and first excited state of the neutral TCNQ, respectively. The $D_2 \leftarrow D_0$ transition at 3.1 eV is an outer-excitation promoting the $1\pi^{*1}$ electron to the higher-lying $2\pi^*$ orbital.

In addition to these experimental studies, there have been a number of theoretical investigations of isolated TCNQ, in both its anion and neutral states.[17-21] The TCNQ radical anion is unusual because it possesses a bound electronic state, a characteristic not commonly associated with anions. In $TCNQ^-$, this arises from a combination of the high binding energy of the excess electron and the conjugated π-system. However, the large size of $TCNQ^-$ and the fact that it contains cyano groups makes the task of performing accurate quantum calculations challenging, particularly in its excited states.

Early *ab-initio* studies focused on the first few excited doublet states of the TCNQ radical anion, which were thought to be bound with respect to the singlet ground state of the neutral, S_0 (^1A_g).[17] Later, Skurski *et al*. calculated the vertical excitation energy of the D_1 (1^2B_{3u}) state to be 1.24 eV above the D_0 ($^2B_{2g}$) ground state,[19] which correlates well with the experimentally observed features in the UV-vis and photodetachment spectra at 1.2 eV. However, calculations involving the higher lying D_2 (2^2B_{3u}) excited state, which corresponds to an outer-excitation, were less consistent with experiment, as some studies determine it to be bound[19] while others predicted it to be unbound[17,21] with respect to the neutral. The experimentally observed $D_2 \leftarrow D_0$ transition occurs at 3.1 eV, so that the second excited D_2 state is unbound by about 0.3 eV, thus highlighting the difficulties involved in accurately calculating electronic excitation energies in large molecules such as $TCNQ^-$.

To probe the electronic structure of TCNQ, we employ photoelectron imaging of the isolated radical anion which, as well as measuring the outgoing electron's kinetic energy, also measures its direction relative to the detachment laser polarisation, providing access the photoelectron angular distributions. In its time-resolved variant, the molecule of interest is excited using an ultrashort pump laser pulse and subsequently, the electron is removed using a second ultrashort probe pulse, which projects the dynamically evolving system onto correlated final states of the neutral. In general, photoelectron spectroscopy has relaxed selection rules. However, final states must be accessible within Koopmans' theorem, which argues that the electronic configuration of the initial state following photodetachment must not change when accessing the final state.[22,23] In the specific case of $TCNQ^-$, the neutral state that TCNQ will be left in, is determined by the electronic structure of the anion state from which the electron is removed. The methodology and application of time-resolved photoelectron spectroscopy has recently been reviewed.[23,24]

Experimental

A detailed description of our experimental apparatus will be presented elsewhere and only an overview is given here. Ions are generated through electrospray ionisation. A 1 mM solution of TCNQ (Sigma-Aldrich) in acetonitrile is pumped at a flow rate of 250 μl hr^{-1} through a stainless steel needle biased at –3 kV. Ions enter a first vacuum region at 3 Torr via a stainless steel capillary heated to 80°C, before passing through an aperture into a second differentially pumped region at 5×10^{-3} Torr. Here, anions are radially confined and axially guided using an ion funnel,[25,26] which also serves as an ion trap by applying a small voltage to an exit aperture. The temperature of the ions within the trap is approximately room temperature (298 K). This leads to a third differentially pumped region at 1×10^{-6} Torr housing a Wiley-McLaren (WM) time-of-flight mass-spectrometer.[27] Anions are injected collinearly into the WM-spectrometer at a 500 Hz repetition rate, which coincides with the repetition rate of the laser system. Anions are accelerated along a 1.3 m field-free drift tube consisting of 3 additional differentially pumped regions, reaching an ultimate pressure of 5×10^{-9} Torr at the point of ion-laser interaction. These additional regions house ion beam steering and ion focusing optics. The anion mass spectrum is monitored using a pair of multi-channel plates (MCPs). The mass spectrum is dominated by a single peak at m/z = 204 amu consisting of approximately 10^3 ions per packet.

Laser pulses are derived from a commercial femtosecond laser system (Spectra-Physics, Spitfire XP-Pro). The fundamental at 795 nm (1.5 eV) is used as a pump in time-resolved experiments and has an associated bandwidth of ~30 nm (~60 meV). Probe pulses are generated by frequency doubling in a type-I Beta-Barium Borate (BBO) crystal. The 398 nm (3.1 eV) pulses are delayed relative to pump pulses using a motorised delay stage (Physik-Instrumente M-505) before being recombined and sent unfocussed into the vacuum chamber through a 1 mm CaF_2 window. The polarisation of the light was set parallel to the electron detector and pulse energies of the pump and probe are typically 120 μJ/pulse and 70 μJ/pulse, respectively. The power densities of both pulses are on the order of $\sim1\times10^{10}$ W cm^{-2} and the temporal width of the pulse pair is determined to be ~120 fs from their cross-correlation in a second BBO crystal.

Photoelectrons are collected using a velocity-map-imaging (VMI) arrangement oriented perpendicularly to the ion beam.[28] The velocity (speed and angle) of the emitted electrons are focused onto a plane, where a position-sensitive detector is placed. In our implementation, the VMI arrangement consists of two μ-metal electrodes and a μ-metal shielded resistive glass tube (Photonis), producing a smooth electric field gradient between the extractor and the grounded electron detector. The position-sensitive detector consists of a pair of MCPs coupled to a phosphor screen (Photek Ltd., VID240). As the amplified electron signal impacts the phosphor screen, light is emitted and collected using a CCD camera (Basler A312f). Raw photoelectron images are typically collected over 10^5 laser shots. Photoelectron spectra (PES) are obtained by subtraction of the azimuthal contribution to the raw image using the polar onion-peeling routine developed in our group,[29] and are calibrated using the well-known PES of Iodide at 266 nm. The energy resolution of the VMI spectrometer was measured to be $\Delta E/E \sim 5$ % or is

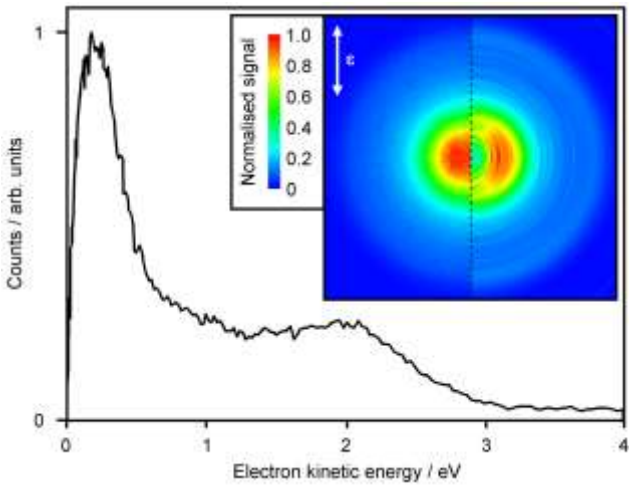

Fig. 2 Photoelectron spectrum of the TCNQ radical anion at 3.1 eV. Inset: raw photoelectron image (left) and the slice through the centre of the deconvoluted electron image (right). The orientation of the laser polarisation vector, ε, is shown in the top left of the image.

limited by the spectral bandwidth of the laser pulses below ~1.2 eV.

Results and discussion

Photoelectron spectrum of $TCNQ^-$ at 3.1 eV

The photoelectron spectrum (PES) of the TCNQ radical anion following detachment at 3.1 eV is presented in Fig. 2, which shows two features centred at 0.2 eV and 2.0 eV. Also shown inset is the raw photoelectron image acquired over 1.75×10^5 laser shots (left half) together with the deconvoluted central slice through the three-dimensional photoelectron cloud (right half). In the PES, the low energy feature corresponds to excitation from the D_0 ground state of the anion to the D_2 state, which promptly autodetaches to the S_0 neutral ground state. This provides a detachment energy of 2.9 eV, which is in good agreement with the measured electron affinity of 2.8 ± 0.1 eV.[14]

The broader kinetic energy feature around 2.0 eV is somewhat unexpected. The photon energy of 3.1 eV is resonant with the D_2 state and as such, this photoelectron peak could be explained in terms of resonance-enhanced two-photon absorption via the D_2 state, which has a large excitation cross-section. However, the D_2 state has a $\pi^2 2\pi^{*1}$ configuration which, in Koopmans' picture, correlates to the neutral in its S_0 state following detachment of an electron from the $2\pi^*$ ($4b_{3u}$) orbital, thus generating photoelectrons around 3.5 eV; this is not observed in the PES.

Theoretical results predict that the D_2 state is not a "pure" state and has contributions from more than one electronic configuration. Skurski *et al*., as well as Brauman and co-workers, calculate that there is a small admixture of the core-excited $\pi^1 1\pi^{*2}$ configuration (8% and 15%, respectively).[15,19] Albeit a small contribution, this core-excited configuration correlates to the T_1 ($^3B_{1u}$) excited state in the neutral following detachment from the $1\pi^*$ ($3b_{2g}$) orbital and we assign the 2.0 eV feature to this process. It is important to note that this core-excited contribution to the D_2 state does not correlate to the S_0 neutral ground state in Koopmans' picture and thus the excess electron does not undergo autodetachment. The measured 2.0 eV provides an estimated energy of ~1.4 eV for the highly spin-forbidden $T_1 \leftarrow S_0$ transition. In an attempt to verify this value, we have measured the absorption spectrum of neutral TCNQ using spectroelectrochemical analysis. However, this shows no absorption in this spectral region indicating that the $T_1 \leftarrow S_0$ transition is optically dark, as expected for a spin-forbidden transition.

The feature around 2.0 eV is much broader than the feature at 0.2 eV. The narrow width of the latter suggests that the potential energy surfaces associated with the D_2 and S_0 are similar and hence, there is little vibrational energy transfer to the neutral following excitation. This is supported by theoretical calculations which suggest that the D_0, D_2 and S_0 all have similar geometries.[19] The lack of major geometric change in going from D_0 to D_2 states is reinforced by the relatively narrow peak at 3.1 eV in the absorption spectrum.[15] This is in contrast to the $D_1 \leftarrow D_0$ transition, which shows clear vibrational progressions, making the observed feature starting at 1.2 eV very broad in the absorption spectrum. The width of the photoelectron feature at 2.0 eV suggests that there is a major geometric change in the photodetachment from the D_2 to T_1 state. This is again in line with theoretical work that calculates the T_1 state to become elongated along the molecular axis with respect to the D_0 and D_2 states due to its additional anti-bonding character.[19] Interestingly, the T_1 state geometry is very similar to that of the D_1. This is evidenced by the PES observed in our time-resolved experiments below.

The integrated intensity of the broad 2.0 eV feature is similar to that of the sharper feature at 0.2 eV, which contradicts the prediction that only a small contribution of the D_2 state is of the core-excited $\pi^1 1\pi^{*2}$ character.[15,19] However, this is not a true reflection on the state contributions, as the cross-section for photodetachment to the T_1 state relative to the S_0 state may be different. Based on our time-resolved spectra discussed below, the cross-section for photodetachment from the $\pi^1 1\pi^{*2}$ configuration to the T_1 state is observed to be comparatively large and can explain the large intensity observed in the 2.0 eV feature.

Excited state relaxation dynamics of $TCNQ^-$

The lifetime and relaxation dynamics following excitation to the D_1 state of $TCNQ^-$ have been studied using time-resolved photoelectron imaging, employing pump and probe pulse energies of 1.5 eV and 3.1 eV, respectively. The pump photon is resonant with the $D_1 \leftarrow D_0$ transition, while the probe removes the excited electron, thus yielding a time-resolved PES. The probe wavelength is chosen to be resonant with the D_2 state so that the feature around 2.0 eV provides a clear signature of the ground state dynamics. The time-resolved PES is shown in Fig. 3a as a normalised false-colour intensity plot where the measured PES have been plotted as a function of pump-probe delay, *t*. To aid in the analysis of the $TCNQ^-$ excited state dynamics and for clarity, individual PES are also presented at three different pump-probe delays in Fig. 3b: *t* =

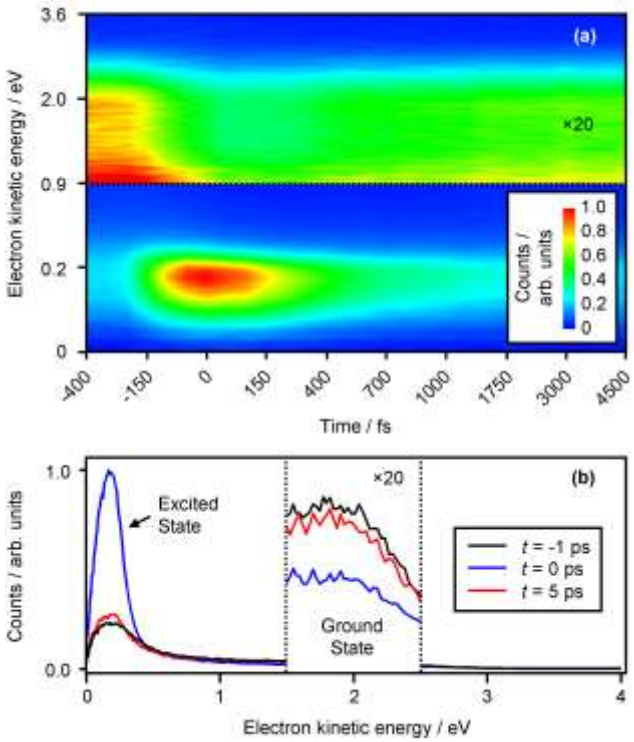

Fig. 3 (a) Normalised false-colour intensity plot of the measured photoelectron spectra as a function of pump-probe delay, *t*, using pump and probe energies of 1.5 eV and 3.1 eV, respectively. (b) Individual photoelectron spectra showing the ground and excited state features at pump-probe delays of $t = -1$, 0 and 5 ps.

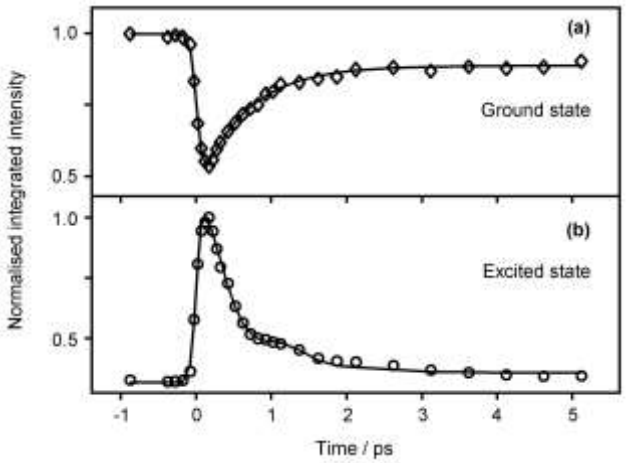

Fig. 4 Integrated intensities of (a) the ground and (b) the excited state features as a function of pump-probe delay, *t*. Solid black lines are fits, as explained in the text.

–1, 0, and 5 ps.

Before the excited state is prepared ($t < 0$), the PES is identical to that in Fig. 2. The pump does not induce any resonance-enhanced two-photon detachment because the D_1 state does not correlate to the S_0 neutral state. This is in contrast to the absorption spectrum measured by Brauman and co-workers, who used a continuous light source.[15] In these experiments a second photon could be absorbed after the excited state has relaxed through internal conversion, producing vibrationally highly excited D_0 ground state. Excitation from the hot D_0 state does correlate to the S_0 and hence, $TCNQ^-$ losses its excess electron. In our case, the excitation pulse is short, such that there is insufficient time for the excited state to undergo internal conversion before absorbing a second photon.

When pump and probe pulses are temporally overlapped, $t = 0$, a large increase in photoelectron signal is observed at 0.2 eV. Additionally, the feature at 2.0 eV is depleted. The latter is a direct measure of the D_0 state population as the only process that can produce photoelectrons at this energy is resonance-enhanced two-photon detachment via the D_2 state. Depletion in this feature indicates that some population has been transferred from the ground state to the excited state. The new feature around 0.2 eV is assigned to the detachment of the excited D_1 state to the T_1 state of the neutral, with which it is correlated in Koopmans' picture. The observed kinetic energy around 0.2 eV is obtained by subtracting the detachment energy and the S_0 to T_1 energy gap from the total photon energy absorbed.

At long time, $t = 5$ ps, the PES indicates that the excited state population has decayed, while a recovery in the ground state is observed.

Exploring the dynamics in further detail, Fig. 4 shows the integrated intensities of the excited and ground state features over the spectral ranges of 0.15 to 0.40 eV and 1.65 to 2.25 eV, respectively. The mirrored dynamics signify that population is transferred from the excited state directly to the ground state, and thus suggests that internal conversion is being observed. We also point out that the excited state feature at 0.2 eV is convoluted with some signal arising from the ground (D_0) state, which will also recover with time. However, because of the relatively large cross-section for detachment from the D_1 state ($D_1 \rightarrow T_1 + e^-$), the dynamics of the ground state contributing to this feature cannot be discerned from the D_1 state dynamics.

The integrated intensity of the ground state peak as a function of pump-probe delay (Fig. 4a, open diamonds) can be fitted using a single exponential function convoluted with the Gaussian instrument response function. The latter describes the temporal cross-correlation of the pump and probe laser pulses. Prior to convolution, the exponential fit function $f(t)$ has the form

$$\begin{aligned} f(t) &= C_0 \,, t < 0 \\ f(t) &= 1 - \left[A_1 \exp(-t/\tau) + C_1\right], t \geq 0 \end{aligned} \,, \qquad (1)$$

where A_1 is the amplitude of the exponential and τ corresponds to the lifetime to the D_1 excited state. The constants C_0 and C_1 represent a measure of the initial ($t < 0$) and final ($t >> 0$) ground state populations, respectively. C_1 is observed to be less than C_0, suggesting that not all the population has recovered and will be discussed later. The fit, shown in Fig. 4a as a solid black line, yields a measured lifetime of 640 ± 50 fs for the ground state population recovery.

The excited state peak dynamics displayed in Fig. 4b as open circles, could also potentially be described by a single exponential fit function. However, such a description does not capture the apparent reduced decay rate around 1 ps. Given

the broad bandwidth of the pump pulse, a coherent superposition of vibrational levels may be excited, leading to coherent nuclear motion of $TCNQ^-$ on the D_1 state. Evidence for nuclear motion can be extracted from the time-resolved PES, which show a small red shift of ~10 meV in the photoelectron peak position at ~500 fs. To account for such dynamics, we have included a periodic modulation of the exponential fit with the resultant functional form

$$g(t) = C_0 \,, t < 0$$
$$g(t) = A_1 \exp(-t/\tau) + A_2 \cos(\omega t + \phi) \exp(-t/\tau_d) + C_1 \,, t \geq 0 \quad (2)$$

before convolution with the Gaussian instrument function. The additional cosine term in $g(t)$ describes a damped oscillation associated with a periodic coherent motion, where A_2 is the amplitude of oscillation, ω is its frequency, ϕ is the initial phase and τ_d is its damping lifetime. In Eq. 2, the constant C_0 accounts for the fact that the spectrum in the 0.2 eV region is composed of contributions from D_1 and D_0 detachment, while C_1 accounts for the offset of the exponential at long time (t = 5 ps). The fit shows that $C_1 \approx C_0$, indicating that the excited state population has almost fully decayed by 5 ps. The resultant fit is shown in Fig. 4b (solid black line) and reproduces the experimental data very well, particularly the deviation from exponential decay observed over the first few picoseconds. The corresponding beat in the ground state is not observed, presumably because of the significantly lower signal levels measured for this feature as evidenced in Fig. 3.

The extracted lifetimes for the excited state decay is 650 ± 70 fs, which correlates exceptionally well with the ground state recovery (640 ± 50 fs) and verifies that the excited state population is directly transferred to the ground state through internal conversion. This highlights the utility of measuring excited and ground state dynamics simultaneously in time-resolved PES. Immediately following internal conversion, the $TCNQ^-$ in its D_0 state is vibrationally highly excited. In order to generate photoelectrons contributing to the high kinetic energy feature (2.0 eV), $TCNQ^-$ must absorb two probe photons, the first of which is resonant with the D_2 state. One may expect there to be differences in the potential energy surfaces of the D_0 and D_2 states and hence, there to be a less favourable Franck-Condon overlap between these two states when the D_0 state is highly excited. Although, the PES at 3.1 eV indicates that the geometries of $TCNQ^-$ in its D_0 and D_2 states are in fact quite similar, small differences in the potential energy surfaces provide an explanation for why the ground state feature does not appear to recover to its initial population. We expect that, as internal vibrational relaxation occurs and energy is redistributed throughout the available vibrational modes of the molecule, the Franck-Condon overlap between the D_0 and D_2 states becomes more favourable again. As a result, a slow recovery of the ground state signal at longer times may be expected.

The fit also provides insight into the nuclear dynamics of the wavepacket on the D_1 state. The wavepacket motion may be isolated from the average decay by subtracting the exponential fit component in Eq. 2 from both the experimental

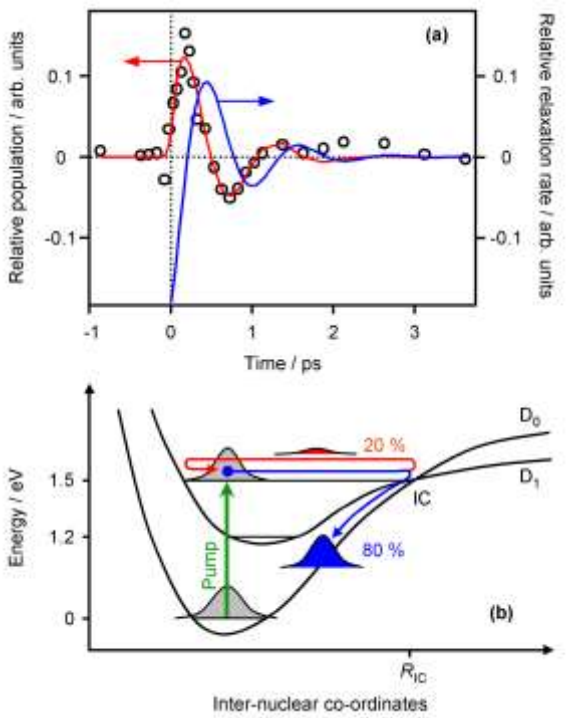

Fig. 5 (a) Isolated oscillatory component of the D_1 excited state population dynamics relative to the average exponential population decay. Open circles represent experimental data and solid red line (left axis) the corresponding fit. Also shown is the relaxation rate relative to the average relaxation rate of the excited state population back to the ground state (solid blue line, right axis). (b) Schematic potential energy curves of the D_1 excited and D_0 ground states of $TCNQ^-$ showing the evolution of the excited state wavepacket (red and blue arrows) following excitation at 1.5 eV (vertical green arrow). R_{IC} is the geometry at which internal conversion can occur.

(open circles) and fit data (solid black line) in Fig. 4b. The resultant wavepacket dynamics are shown in Fig. 5a (open circles and red line correspond to the experimental and fit data, respectively). Positive signal indicates that there is more population in the excited state relative to the population of the D_1 state if it was decaying purely exponentially. Conversely, negative signal correlates to a depletion of population relative to the exponential decay. In addition to the relative populations, we may also gain insight into the decay rate relative to the average rate. This is shown by the blue line in Fig. 5a, which corresponds to the negative gradient of the oscillatory cosine component in Eq. 2, where we have omitted the convolution with the instrument function for clarity. Positive signal corresponds to an enhanced rate and negative to a reduced decay rate, relative to the average rate of $(650 \text{ fs})^{-1}$.

The dynamics are occurring on a multi-dimensional potential energy surface. The period of the oscillation is 1.1 ps, corresponding to a vibrational energy spacing of ~30 cm^{-1}. In principle, it may be possible to assign the oscillation frequency to specific modes of $TCNQ^-$ in the D_1 state although such an analysis is beyond the scope of this article. A schematic representation of the dynamics is presented in Fig. 5b.

The initial phase of the wavepacket dynamics provides some information about the relative geometry of $TCNQ^-$ at;

(1) the point where it undergoes internal conversion and (2) the ground state geometry in which the D_1 state is initially prepared. A phase of $\phi = -1.1$ radians is extracted from the fit to Eq. 2. In terms of the relative rate of relaxation, this corresponds to a reduced rate when the wavepacket is formed, indicating that the Franck-Condon excitation region occurs at a geometry which differs from that required for the internal conversion to take place. However, the relative rate is also increasing (positive gradient) at $t = 0$, indicating that the Franck-Condon region is not precisely at the inner turning point. It also shows that the wavepacket is initially moving towards the internal conversion geometry (R_{IC}) on the D_1 state.

The relative relaxation rate reaches a maximum at ~430 fs, at which time the internal conversion rate between the D_1 and D_0 states is maximised. A comparison of the relative populations at $t = 150$ fs and $t = 1.3$ ps suggests that approximately 80 % of the wavepacket is transferred back to the ground state when the wavepacket samples the internal conversion geometry for the first time (blue wavepacket in Fig. 5b), leaving only ~20 % in the excited state (red wavepacket). This may indicate that the coupling between the D_1 and D_0 states is particularly strong, however, this is not definitive as it also depends on the momentum initially imparted to the wavepacket on the D_1 excited state.[31] The remainder of the wavepacket on the D_1 state then propagates away from R_{IC}, as indicated by the reduction in the relative rate of relaxation. The wavepacket reaches the inner turning point at ~980 fs, before returning to R_{IC} at ~1.5 ps. After this time, the overall fit becomes poor. This could be due to more complicated dynamics occurring on the excited state or because of the much reduced signal levels as most of the D_1 population has decayed. Regardless, the coherent oscillation is mostly damped out after one period, indicating that most of the population is transferred back to the D_0 state as the wavepacket reaches the internal conversion geometry for the first time.

It is worth noting that similar wavepacket dynamics have been observed in time-resolved fluorescence up-conversion studies conducted on related tetracyanoethylene (TCNE) based CT complexes in the condensed phase.[32,33] In these studies the neutral CT complex is excited to the charge-separated state ($donor^+$-$TCNE^-$) and the subsequent relaxation dynamics are monitored. A single vibrational frequency is observed which is independent of the donor molecule used in the CT complexes. This observation led to the conclusion that an intramolecular mode in the TCNE alone drives the relaxation dynamics of the complex. Clearly, the isolated dynamics of acceptor molecules in CT complexes is important, and it would be of interest if similar dynamics could be observed in the relaxation of TCNQ containing CT complexes.

For completeness, we also consider the reverse dynamics, which may be observed in our time-resolved experiments by changing the labels on pump and probe. In this case, we might expect to observe dynamics following excitation at 3.1 eV and probing at 1.5 eV, which should reflect the dynamics of the excited D_2 state. As noted above, the D_2 state is of mixed core- and outer-excited character. When probed at 1.5 eV, the latter, $\pi^2 2\pi^{*1}$ configuration, would correlate to the S_0 neutral state, leading to photoelectrons in the 1.8 eV range when $t < 0$. Additionally, we may expect to see depletion in the 0.2 eV region. However, we do not observe such dynamics. If the core-excited $\pi^1 1\pi^{*2}$ character of the D_2 state were probed, detachment would produce neutral TCNQ in the T_1 state yielding photoelectrons around 0.2 eV. Note that this character is likely to be long lived as it does not correlate with the S_0 ground state of the neutral and hence cannot readily autodetach. Alternatively, one may expect internal conversion to the D_1 or D_0 states, however, we have observed no obvious dynamics in the reverse direction.

Conclusions

In summary, we have measured the photoelectron spectrum of $TCNQ^-$ at 3.1 eV, which corroborates the prediction that the D_2 state has mixed character, provides some insight into the relative potential energy surfaces of the excited states of the anion and neutral and provides a measure of the optically forbidden $T_1 \leftarrow S_0$ transition energy of the neutral. Additionally, time-resolved PES show that the D_1 excited state undergoes internal conversion back to the D_0 ground state with a lifetime of 650 fs. This is however an average value and a detailed analysis of the dynamics show that coherent nuclear motion can be observed on the excited state with a ~30 cm^{-1} frequency. At 430 fs, the wavepacket reaches the geometry at which $TCNQ^-$ in the D_1 state internally converts to the D_0 state with an ~80 % efficiency.

TCNQ and its derivatives remain a very active research area. The results presented here provide a molecular level understanding of the electronic structure and energy flow in this fundamental CT acceptor. Such detailed knowledge of the molecular building blocks on which a vast number of materials are based is a prerequisite to the design, development and understanding of materials with tailor-made properties, such as organic metals, non-linear optics and liquid crystal devices.

Acknowledgements

We are grateful to Durham University and the EPSRC for funding under grant EP/D073472/1.

Notes and references

[a] *Department of Chemistry, University of Durham, South Road, Durham, UK DH1 3LE; E-mail: j.r.r.verlet@durham.ac.uk*

1 L. R. Melby, W. Mahler, W. E. Mochel, R. J. Harder, W. R. Hertler and R. E. Benson, *J. Am. Chem. Soc.*, 1962, **84**, 3374.
2 W. J. Siemons, P. E. Biersted and R. G. Kepler, *J. Chem. Phys.*, 1963, **39**, 3523.
3 G. L. Closs and J. R. Miller, *Science*, 1988, **240**, 440.
4 D. Jerome, *Chem. Rev.*, 2004, **104**, 5565.
5 J. Ferraris, D. O. Cowan, V. Walatka and J. H. Perlstein, *J. Am. Chem. Soc.*, 1973, **95**, 948.
6 J. B. Torrance, *Acc. Chem. Res.*, 1979, **12**, 79.
7 R. C. Wheland and J. L. Gillson, *J. Am. Chem. Soc.*, 1976, **98**, 3916.
8 J. L. Segura and N. Martin, *Angew. Chem. Int. Ed.*, 2001, **40**, 1372.

9 D. F. Perepichka, M. R. Bryce, C. Pearson, M. C. Petty, E. J. L. McInnes and J. P. Zhao, *Angew. Chem. Int. Ed.*, 2003, **42**, 4636.
10 H. Okamoto, K. Ikegami, T. Wakabayashi, Y. Ishige, J. Togo, H. Kishida and H. Matsuzaki, *Phys. Rev. Lett.*, 2006, **96**.
11 J. M. Cole, R. C. B. Copley, G. J. McIntyre, J. A. K. Howard, M. Szablewski and G. H. Cross, *Phys. Rev. B*, 2002, **65**, 125107.
12 L. O. Palsson, M. Szablewski, A. Roberts, A. Masutani, G. D. Love, G. H. Cross, D. Bloor, A. J. Kay, A. D. Woolhouse, A. Masutani and A. Yasuda, *Mol. Cryst. Liq. Cryst.*, 2003, **402**, 279.
13 D. Bloor, Y. Kagawa, M. Szablewski, M. Ravi, S. J. Clark, G. H. Cross, L. O. Palsson, A. Beeby, C. Parmer and G. Rumbles, *J. Mater. Chem.*, 2001, **11**, 3053.
14 C. E. Klots, R. N. Compton and V. F. Raaen, *J. Chem. Phys.*, 1974, **60**, 1177.
15 E. A. Brinkman, E. Gunther, O. Schafer and J. I. Brauman, *J. Chem. Phys.*, 1994, **100**, 1840.
16 I. Haller and F. B. Kaufman, *J. Am. Chem. Soc.*, 1976, **98**, 1464.
17 I. Zanon and C. Pecile, *J. Phys. Chem.*, 1983, **87**, 3657.
18 V. G. Zakrzewski, O. Dolgounitcheva and J. V. Ortiz, *J. Chem. Phys.*, 1996, **105**, 5872.
19 P. Skurski and M. Gutowski, *J. Mol. Struct. (THEOCHEM)*, 2000, **531**, 339.
20 M. Sobczyk, P. Skurski and J. Simons, *J. Phys. Chem. A*, 2003, **107**, 7084.
21 M. Makowski and M. T. Pawlikowski, *Int. J. Quantum Chem.*, 2006, **106**, 1736.
22 V. Blanchet, M. Z. Zgierski, T. Seideman and A. Stolow, *Nature*, 1999, **401**, 52.
23 A. Stolow, A. E. Bragg and D. M. Neumark, *Chem. Rev.*, 2004, **104**, 1719.
24 J. R. R. Verlet, *Chem. Soc. Rev.*, 2008, **37**, 505.
25 S. A. Shaffer, D. C. Prior, G. A. Anderson, H. R. Udseth and R. D. Smith, *Anal. Chem.*, 1998, **70**, 4111.
26 T. Wyttenbach, P. R. Kemper and M. T. Bowers, *Int. J. Mass Spectrom.*, 2001, **212**, 13.
27 W. C. Wiley and I. H. Mclaren, *Rev. Sci. Instrum.*, 1955, **26**, 1150.
28 A. T. J. B. Eppink and D. H. Parker, *Rev. Sci. Instrum.*, 1997, **68**, 3477.
29 G. M. Roberts, J. L. Nixon, J. Lecointre, E. Wrede and J. R. R. Verlet, *Rev. Sci. Instrum.*, 2009, **80**, 053104.
30 R. Mabbs, E. R. Grumbling, K. Pichugin and A. Sanov, *Chem. Soc. Rev.*, 2009, **38**, 2169.
31 C. Wittig, *J. Phys. Chem. B*, 2005, **109**, 8428.
32 I. V. Rubtsov and K. Yoshihara, *J. Phys. Chem. A*, 1997, **101**, 6138.
33 I. V. Rubtsov and K. Yoshihara, *J. Phys. Chem. A*, 1999, **103**, 10202.